Available online at www.sciencedirect.com
SCIENCE DIRECT®
International Journal of Rock Mechanics & Mining Sciences 41 (2004) 613–628
International Journal of Rock Mechanics and Mining Sciences
www.elsevier.com/locate/ijrmms

A generalized solution for tetrahedral rock wedge stability analysis

Zuyu Chen*

Department of Hydraulic Engineering, Tsinghua University, China Institute of Water Resources and Hydropower Research, 20, West Chegongzhuang Road, P.O. Box 366, Beijing 100044, China

Accepted 28 December 2003

Abstract

It has been found that the limit equilibrium approach commonly used for tetrahedral rock wedge stability analysis is statically indeterminate and the conventional method proposed in textbooks actually involves an assumption that the shear forces applied on the failure planes are parallel to the line of intersection. A new method that allows an input of various shear force directions is presented in this paper. This method starts from an assumed wedge displacement vector that can be related to the shear force directions. By applying the limit equilibrium conditions a governing equation calculating the factor of safety has been obtained. This equation also permits a formal demonstration to confirm that a maximum factor of safety exists when the rock wedge dilates at values of friction angles to the left and right failure planes respectively, the direction required Mohr–Coulomb's associative flow law. The generalized method therefore provides a theoretical support to some fundamental postulates in Plasticity. The factors of safety obtained by the conventional method and the generalized approach are not substantially different if the shear strength of the failure planes involves a reasonable value of cohesion. However the deviations between the two approaches can be remarkable if the material is purely frictional. Further study by physical model testing and field investigation is recommended.

1. Introduction

Wedge failure is common in rock slopes. The simplest and most frequently encountered failure mode involves a tetrahedral unstable rock mass that slips along two weak planes as shown in Fig. 1. In general, a tetrahedral wedge failure is prone to occur if the line of intersection of the two planes daylights at the slope surface.

The limit equilibrium method is commonly used to find the factor of safety for this kind of failure mode. The procedures are well documented in the literature [1–3].

However, a detailed study of these procedures will realize that the problem is statically indeterminate. In the established force equilibrium equations, there are generally two unknown internal force vectors applied on the two failure surfaces, which involve a total of six components in the x, y, z co-ordinate system (Fig. 1). The factor of safety to be evaluated adds one more. The number of available force equilibrium equations for the wedge block, normally expressed by the projection of forces on the co-ordinate axes, is three. Another two available equations can be provided by Mohr–Coulomb failure criterion that relates the magnitude of the normal and shear forces on the failure surfaces. Therefore, two assumptions must be made to allow the problem to be statically determinate. The traditional method presented in textbooks actually assumes that the shear forces on the failure surfaces are parallel to the line of intersection of the two failure surfaces.

Perhaps, Pan [4] was the first one who argued the theoretical background of the conventional method. He believed that when a landslide is imminent, the internal forces would be reorganized to mobilize maximum resistance against failure. Based on this understanding, Pan put forward his 'principle of minimum and maximum' as follows:

- Among many possible slip surfaces, the real one offers the minimum resistance against failure (principle of minimum).
- For a specified slip surface, the stress in the failure mass as well on the slip surface will be reorganized to develop the maximum resistance against failure (principle of maximum).

*Tel.: 86-10-685-148-24; fax: 86-10-684-383-17.
E-mail address: chenzy@tsinghua.edu.cn (Z. Chen).

1365-1609/$ - see front matter © 2004 Elsevier Ltd. All rights reserved.
doi:10.1016/j.ijrmms.2003.12.150

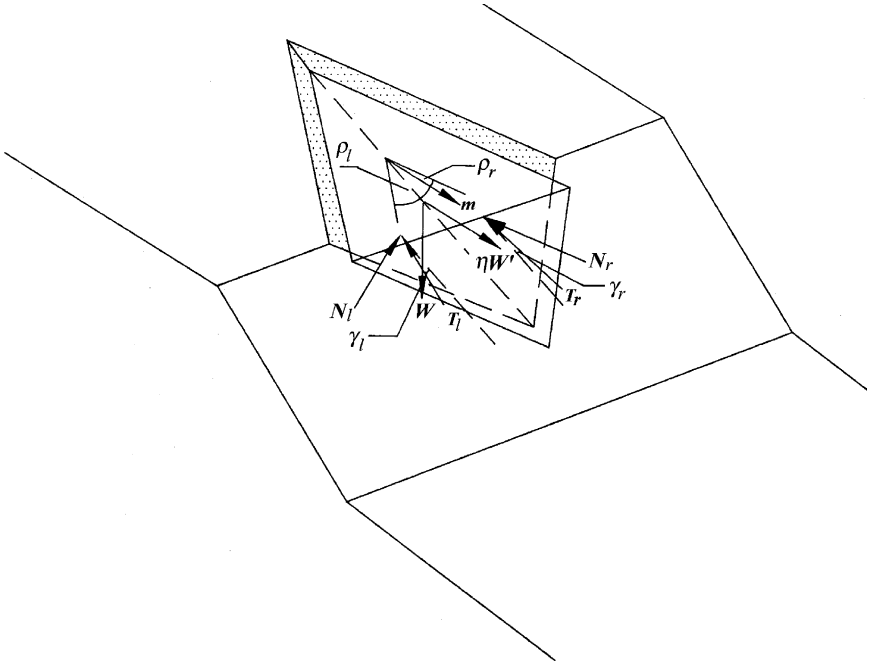

Fig. 1. The rock wedge failure. *Legend for the vectors*: $\boldsymbol{m}$ is the direction of the wedge movement, $\boldsymbol{N}_l$, $\boldsymbol{N}_r$ the normal of the failure planes, $\boldsymbol{T}_l$, $\boldsymbol{T}_r$ the shear forces on the failure planes, $\boldsymbol{W}$ the external force, $\eta \boldsymbol{W}'$ the disturbance force that brings about the failure. The subscripts 'l' and 'r' stand for the left and right planes, respectively.

Chen [5] indicated that Pan's Principle could actually be derived from the Upper and Lower Bound Theorems of Plasticity.

To understand the impact of this argument, let us examine an example that has a symmetric geometry and material properties with respect to the line of intersection, as shown in Table 1 [6]. The cohesion of the two failure surfaces is set to zero. The angle between the line of intersection and the shear force applied on the failure surface is denoted by γ. For this symmetric wedge with simple geometry, it is possible to establish a formulation to calculate F associated with different values of γ. The case $\gamma = 0^\circ$ corresponds to the conventional method and gives a value of factor of safety $F = 0.727$. However F increases as γ becomes larger and eventually reaches a maximum of 1.002 at $\gamma = 42.5^\circ$ (Fig. 2).

A further study was carried out by the method using the Upper Bound Theorem of Plasticity [6] (refer to the appendix). By assigning a plastic wedge displacement that inclines at an angle of $\rho = 27.5^\circ$, being equal to the friction angle ϕ for both the left and right failure planes, the work-energy balance equation gave an F that was exactly the maximum of 1.002. Also it was found that '$\rho = \phi = 27.5^\circ$' exactly corresponds to '$\gamma = 42.5^\circ$' (described in detail in Sections 2.2 and 2.3). This means that the wedge obtains its maximum factor of safety when it moves in a direction that a Mohr–Coulomb's associative material exhibits. If this coincidence represents a common behavior, Pan's 'principle of maximum' can thus be supported by the Upper Bound Theorem in plasticity, and a solution other than the traditional one in wedge failure analysis should really be considered seriously in our profession.

Table 1
Parameters for an example of symmetric wedge

Surface	Dip direction	Dip angle	Friction angle	Cohesion
Left	120°	67.2°	27.5°	0
Right	240°	67.2°	27.5°	0
Crest	180°	0°		
Slope	180°	90°		

Note: Height = 100 m, Unit weight = 2.7×9.8 kN/m^3.

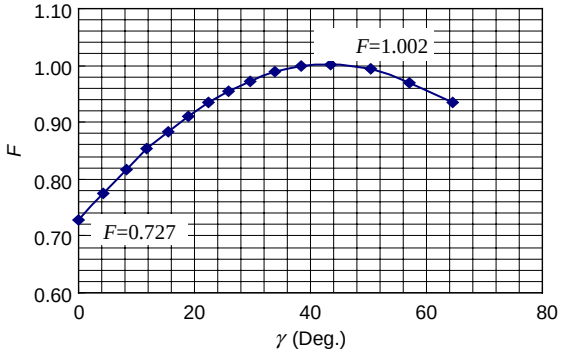

Fig. 2. Relationships between the factor of safety F and the shear force inclination γ for the example described in Table 1.

The purposes of this paper are:

(1) to present a generalized solution to wedge failure analysis which allows input of any specified shear force directions on the failure planes;
(2) to demonstrate that a maximum factor of safety does exist when the wedge deforms in compliance with the Mohr–Coulomb's associative flow law;
(3) to discuss the theoretical and practical implications of the findings described in this paper.

2. Background

2.1. Definition of the disturbance factors

For a soil or rock slope, the factor of safety F is defined to be a coefficient that reduces the available shear strength parameters c and ϕ to c_e and ϕ_e, which bring the wedge to a limiting equilibrium:

$$c_e = c/F, \tag{1}$$

$$\tan\phi_e = \tan\phi/F. \tag{2}$$

Consequently the following relationship applies:

$$T = c_e A + N\tan\phi_e, \tag{3}$$

where N and T are effective normal and shear forces on the failure surface, respectively, and A is the area of the failure plane.

Sarma [7] suggested an alternative approach which involves a horizontal force $\eta \boldsymbol{W}'$ applied to the whole failure mass. This gives rise to the limit equilibrium state where η is called critical acceleration coefficient and $\boldsymbol{W}'$ represents a disturbance force whose magnitude is the weight of the failure mass. The main advantage of using this approach is that η can normally be determined by a straightforward equation without the need for iteration. Sarma's approach also has an important feature in that it brings the failure mechanism by loading rather than the reduction of strength parameters, and consequently renders an access to the framework of plasticity as will be discussed subsequently. In wedge analysis where the three-dimensional effect is of concern, the horizontal disturbance force is further defined as having the same dip direction as that of the line of intersection, designated $\boldsymbol{j}$.[1] That is, $\eta \boldsymbol{W}'$ and $\boldsymbol{j}$ constitute a vertical plane.

It is possible to transfer the values of η to a solution for factor of safety normally required in engineering practice. By finding η for a series of c_e and ϕ_e values related to different values of F, the solution for F, which is associated with $\eta = 0$, can then be found by interpolation.

2.2. The concept of identical directions of shear force and displacement

A basic relationship that relates the directions of shear force and shear displacement (or velocity) on a failure plane (hereafter referred to as 'concept of identical shear directions') is introduced here.

It is stated that on a failure plane, shear displacement takes place in the same direction in which the shear force is applied. As has been discussed by Chen et al. [8], the Mohr–Coulomb's failure law requires that the shear failure surface is perpendicular to the plane constituted by the major and minor principal shear stresses (refer to Fig. 3). This means that no shear displacement will develop in the directions in which the intermediate principal stress applies.

Neglecting the shear strain component in the direction perpendicular to the plane constituted by the normal and shear forces on a shear failure plane is a common approach for all 3D limit analysis methods. With this argument, Drescher and Kang [9] were able to confirm that in the 3D space, the energy dissipation D developed on a shear plane can be determined by the same expression as that for the 2D areas for Mohr–Coulomb's associative material [10], i.e.,

$$D = Vc\cos\phi\, A, \tag{4}$$

where V is the plastic velocity on the failure plane. Subsequent publications based on this equation include the work by Michalowski [11], Lin and Drescher [12], and Chen et al. [8].

It should be noted that in the framework of limit analysis, the elastic strain is considered much smaller than plastic strain and is neglected. The plastic velocity V is regarded as the entire physical displacement rate of the wedge as well.

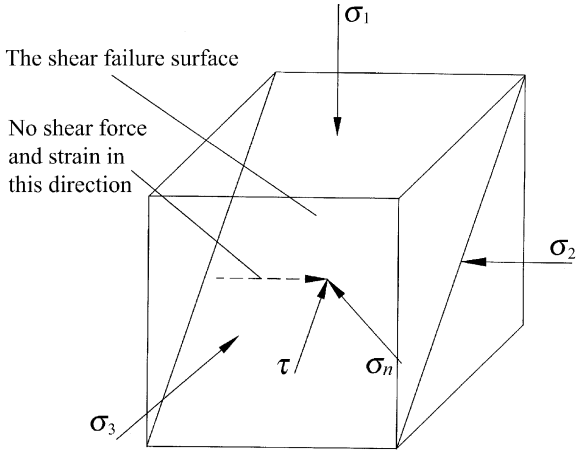

Fig. 3. The 'concept of identical shear directions'.

[1] In this paper an italic capital letter printed in bold and in regular forms represent a vector and its magnitude, respectively. A vector printed in lower case means a unit vector.

With this concept, one is able to establish a relationship between γ and ρ, to be described in detail in the subsequent section. In the example shown in the Introduction, this concept enabled us to confirm that '$\gamma = 42.5°$' corresponds to '$\rho = 27.5°$'. Introducing this concept is therefore of prime significance to the success of the formulations presented in this paper.

2.3. Mathematical representations for various vectors

It has been found that representing a vector by a linear combination of several independent vectors will greatly facilitate the mathematical derivation required in this work.

(1) *The line of intersection*. The unit vector of line of intersection of the two planes, denoted by $\boldsymbol{j}$, is perpendicular to $\boldsymbol{n}_\mathrm{l}$ and $\boldsymbol{n}_\mathrm{r}$, the inward normals of the two planes. Therefore it can be expressed as

$$\boldsymbol{j} = \boldsymbol{n}_\mathrm{l} \times \boldsymbol{n}_\mathrm{r}/\Delta, \tag{5}$$

where Δ is magnitude of $\boldsymbol{n}_\mathrm{l} \times \boldsymbol{n}_\mathrm{r}$, a coefficient that makes $\boldsymbol{j}$ be unit. Defining θ to be the angle between $\boldsymbol{n}_\mathrm{l}$ and $\boldsymbol{n}_\mathrm{r}$, the following relationships apply:

$$\Delta = \sin\theta, \tag{6}$$

$$\cos\theta = \boldsymbol{n}_\mathrm{l} \cdot \boldsymbol{n}_\mathrm{r}. \tag{7}$$

Also we have

$$\left.\begin{aligned} \boldsymbol{j} \cdot \boldsymbol{n}_\mathrm{l} = 0 \\ \boldsymbol{j} \cdot \boldsymbol{n}_\mathrm{r} = 0 \end{aligned}\right\} \tag{8}$$

(2) *Displacement vector of the wedge block*. The unit displacement vector of the wedge block, designated $\boldsymbol{m}$, is defined to incline at angles of ρ_l and ρ_r to the left and right planes, respectively. It can be represented by vectors $\boldsymbol{j}$, $\boldsymbol{n}_\mathrm{l}$, and $\boldsymbol{n}_\mathrm{r}$ as follows:

$$\boldsymbol{m} = a_m\boldsymbol{j} + b_m\boldsymbol{n}_\mathrm{l} + c_m\boldsymbol{n}_\mathrm{r}, \tag{9}$$

where a_m, b_m, and c_m are coefficients that will be determined based on $\boldsymbol{\rho}_\mathrm{l}$ and $\boldsymbol{\rho}_\mathrm{r}$.

(3) *Shear force vectors for the left and right planes*. Once $\boldsymbol{m}$ is determined, the unit shear force vector on the left and right planes, designated $\boldsymbol{T}_\mathrm{l}$ and $\boldsymbol{T}_\mathrm{r}$, can be determined based on the 'concept of identical shear directions'. Fig. 4(a) shows a vector triangle that is illustrated in a cross section constituted by $\boldsymbol{m}$ and $\boldsymbol{n}_\mathrm{l}$. The unit vector of $\boldsymbol{T}_\mathrm{l}$, designated $\boldsymbol{t}_\mathrm{l}$, can be determined by

$$\boldsymbol{t}_\mathrm{l} = -\boldsymbol{m}\sec\rho_\mathrm{l} + \boldsymbol{n}_\mathrm{l}\tan\rho_\mathrm{l}. \tag{10}$$

Similarly for the right plane, we have

$$\boldsymbol{t}_\mathrm{r} = -\boldsymbol{m}\sec\rho_\mathrm{r} + \boldsymbol{n}_\mathrm{r}\tan\rho_\mathrm{r}. \tag{11}$$

(4) *The 'combined friction force' for the left and right planes*. The internal force applied on a failure planes is divided into two parts as shown in Fig. 5 which is illustrated in a cross section constituted by $\boldsymbol{m}$ and the normals of the two failure planes. The first part refers to the cohesion force designated $\boldsymbol{C}_\mathrm{l}$ (or $\boldsymbol{C}_\mathrm{r}$), whose magnitude is $c_{\mathrm{el}}A_\mathrm{l}$ (or $c_{\mathrm{er}}A_\mathrm{r}$). This part of internal force does not contain unknown variables except the value of F, if the 'factor of safety approach' is employed. The second one, designated $\boldsymbol{P}_\mathrm{l}$ (or $\boldsymbol{P}_\mathrm{r}$), is the resultant of the normal force $\boldsymbol{N}_\mathrm{l}$ (or $\boldsymbol{N}_\mathrm{r}$) and the friction force under the application of the normal force. Obviously, $\boldsymbol{P}_\mathrm{l}$ and $\boldsymbol{P}_\mathrm{r}$ are inclined at ϕ_l and ϕ_r to the normal of the left and right planes, respectively. Since $\boldsymbol{P}_\mathrm{l}$ and $\boldsymbol{P}_\mathrm{r}$ will appear frequently later, they are referred to as 'combined friction forces' hereafter.

The unit 'combined friction force' vector on a plane is also represented by the linear combination of $\boldsymbol{m}$, $\boldsymbol{n}_\mathrm{l}$, and

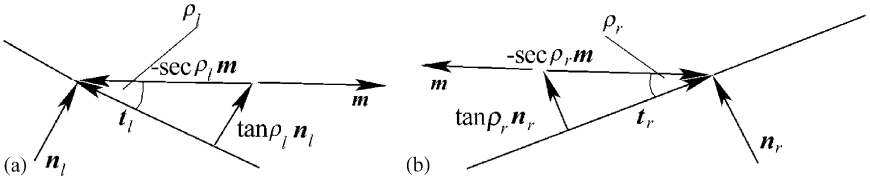

Fig. 4. Combinations of vectors for the shear forces: (a) representing $\boldsymbol{t}_\mathrm{l}$ by $\boldsymbol{m}$ and $\boldsymbol{n}_\mathrm{l}$ and (b) representing $\boldsymbol{t}_\mathrm{r}$ by $\boldsymbol{m}$ and $\boldsymbol{n}_\mathrm{r}$.

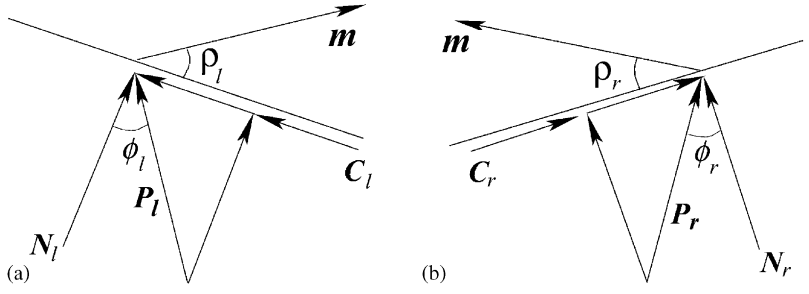

Fig. 5. The 'Combined friction force' vector: (a) the left plane and (b) the right plane.

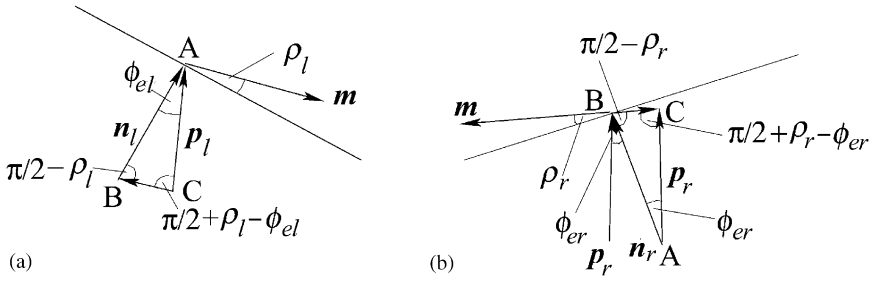

Fig. 6. Combinations of vectors for the 'Combined friction forces': (a) representing $\boldsymbol{p}_\mathrm{l}$ by $\boldsymbol{m}$ and $\boldsymbol{n}_\mathrm{l}$ and (b) representing $\boldsymbol{p}_\mathrm{r}$ by $\boldsymbol{m}$ and $\boldsymbol{n}_\mathrm{r}$.

$\boldsymbol{n}_\mathrm{r}$. From the vector triangle shown in Fig. 6(a), illustrated in a cross section constituted by the $\boldsymbol{m}$ and $\boldsymbol{n}_\mathrm{l}$, it can be shown that

$$\frac{\overline{\mathrm{AB}}}{\sin(\frac{\pi}{2}+\rho_\mathrm{l}-\phi_\mathrm{el})}=\frac{\overline{\mathrm{BC}}}{\sin\phi_\mathrm{el}}=\frac{\overline{\mathrm{CA}}}{\sin(\frac{\pi}{2}-\rho_\mathrm{l})}, \tag{12}$$

where the magnitude of $\overline{\mathrm{CA}}$ is unity. Therefore $\boldsymbol{p}_\mathrm{l}$, the unit vector of 'combined friction force' on the left plane, is

$$\boldsymbol{p}_\mathrm{l}=-\overline{\mathrm{BC}}\boldsymbol{m}+\overline{\mathrm{AB}}\boldsymbol{n}_\mathrm{l}=-\frac{\sin\phi_\mathrm{el}}{\cos\rho_\mathrm{l}}\boldsymbol{m}+\frac{\cos(\rho_\mathrm{l}-\phi_\mathrm{el})}{\cos\rho_\mathrm{l}}\boldsymbol{n}_\mathrm{l}. \tag{13}$$

Similarly we have

$$\boldsymbol{p}_\mathrm{r}=-\frac{\sin\phi_\mathrm{er}}{\cos\rho_\mathrm{r}}\boldsymbol{m}+\frac{\cos(\rho_\mathrm{r}-\phi_\mathrm{er})}{\cos\rho_\mathrm{r}}\boldsymbol{n}_\mathrm{r}. \tag{14}$$

(5) *The external force vector of the wedge block*. The resultant of the wedge weight, external loads and pore pressures applied on the two planes is denoted by $\boldsymbol{W}$, with its unit vector of $\boldsymbol{w}$. The pore pressures are known constants and hence not explicitly separated from $\boldsymbol{W}$ for brevity. The unit external force $\boldsymbol{w}$ is represented by

$$\boldsymbol{w}=a_w\boldsymbol{m}+b_w\boldsymbol{n}_\mathrm{l}+c_w\boldsymbol{n}_\mathrm{r}. \tag{15}$$

Similarly, Sarma's disturbance force vector $\boldsymbol{w}'$ is represented by

$$\boldsymbol{w}'=a_{w'}\boldsymbol{m}+b_{w'}\boldsymbol{n}_\mathrm{l}+c_{w'}\boldsymbol{n}_\mathrm{r}. \tag{16}$$

The coefficients of a, b, and c with the various subscripts involved in Eqs. (15) and (16) will be determined subsequently.

(6) *Basic relationships*. It is well known from the theory of vector analysis that

$$\boldsymbol{a}\cdot(\boldsymbol{b}\times\boldsymbol{c})=(\boldsymbol{a}\times\boldsymbol{b})\cdot\boldsymbol{c}=\boldsymbol{b}\cdot(\boldsymbol{c}\times\boldsymbol{a}), \tag{17}$$

$$\boldsymbol{a}\cdot(\boldsymbol{a}\times\boldsymbol{c})=0, \tag{18}$$

$$\boldsymbol{a}\cdot(\boldsymbol{b}\times\boldsymbol{a})=0, \tag{19}$$

$$\boldsymbol{a}\times\boldsymbol{a}=0, \tag{20}$$

$$\boldsymbol{a}\cdot\boldsymbol{a}=|\boldsymbol{a}|^2, \tag{21}$$

where $\boldsymbol{a}$, $\boldsymbol{b}$, and $\boldsymbol{c}$ are arbitrary vectors.

These expressions will greatly facilitate the mathematical derivations shown in Section 3 and permit the following relationships to apply:

(1) For $\boldsymbol{m}$, we have from Eq. (9)

$$\begin{aligned}|\boldsymbol{m}|^2&=(a_m\boldsymbol{j}+b_m\boldsymbol{n}_\mathrm{l}+c_m\boldsymbol{n}_\mathrm{r})\cdot(a_m\boldsymbol{j}+b_m\boldsymbol{n}_\mathrm{l}+\boldsymbol{c}_m\boldsymbol{n}_\mathrm{r})\\&=a_m^2+b_m^2+2b_mc_m\cos\theta+c_m^2=1,\end{aligned} \tag{22}$$

$$\left.\begin{aligned}\boldsymbol{m}\cdot\boldsymbol{n}_\mathrm{l}&=\sin\rho_\mathrm{l}=b_m+c_m\cos\theta\\\boldsymbol{m}\cdot\boldsymbol{n}_\mathrm{r}&=\sin\rho_\mathrm{r}=b_m\cos\theta+c_m\end{aligned}\right\} \tag{23}$$

Therefore b_m and c_m can be determined by

$$b_m=\frac{\sin\rho_\mathrm{l}-\cos\theta\sin\rho_\mathrm{r}}{\sin^2\theta}, \tag{24}$$

$$c_m=\frac{\sin\rho_\mathrm{r}-\cos\theta\sin\rho_\mathrm{l}}{\sin^2\theta}. \tag{25}$$

Substituting Eqs. (24) and (25) into Eq. (22), through a straightforward but lengthy derivation one obtains

$$\begin{aligned}a_m=\boldsymbol{m}\cdot\boldsymbol{j}&=\mathrm{cosec}\,\theta\\&\quad\times\sqrt{\sin^2\theta-\sin^2\rho_\mathrm{r}-\sin^2\rho_\mathrm{l}+2\sin\rho_\mathrm{l}\sin\rho_\mathrm{r}\cos\theta}.\end{aligned} \tag{26}$$

(2) For $\boldsymbol{w}$, we have

$$\left.\begin{aligned}\boldsymbol{w}\cdot\boldsymbol{n}_\mathrm{l}&=a_w\sin\rho_\mathrm{l}+b_w+c_w\cos\theta\\\boldsymbol{w}\cdot\boldsymbol{n}_\mathrm{r}&=a_w\sin\rho_\mathrm{r}+b_w\cos\theta+c_w\end{aligned}\right\} \tag{27}$$

in which $\boldsymbol{w}\cdot\boldsymbol{n}_\mathrm{l}$ and $\boldsymbol{w}\cdot\boldsymbol{n}_\mathrm{r}$ are known, being independent of F, ρ_l and ρ_r. From Eq. (27), we have

$$\begin{aligned}b_w&=(\boldsymbol{w}\cdot\boldsymbol{n}_\mathrm{l}-\boldsymbol{w}\cdot\boldsymbol{n}_\mathrm{r}\cos\theta)\,\mathrm{cosec}^2\,\theta\\&\quad+(\sin\rho_\mathrm{r}\cos\theta-\sin\rho_\mathrm{l})\,\mathrm{cosec}^2\,\theta a_w,\end{aligned} \tag{28}$$

$$\begin{aligned}c_w&=(\boldsymbol{w}\cdot\boldsymbol{n}_\mathrm{r}-\boldsymbol{w}\cdot\boldsymbol{n}_\mathrm{l}\cos\theta)\,\mathrm{cosec}^2\,\theta\\&\quad+(\sin\rho_\mathrm{l}\cos\theta-\sin\rho_\mathrm{r})\,\mathrm{cosec}^2\,\theta a_w.\end{aligned} \tag{29}$$

a_w can be determined by the following relationship:

$$\boldsymbol{w}\cdot\boldsymbol{j}=a_w\boldsymbol{m}\cdot\boldsymbol{j}=a_wa_m \tag{30}$$

from which a_w is calculated by

$$a_w = \frac{\boldsymbol{w}\cdot\boldsymbol{j}}{a_m} = \frac{\boldsymbol{w}\cdot\boldsymbol{j}}{\operatorname{cosec}\theta\sqrt{\sin^2\theta-\sin^2\rho_r-\sin^2\rho_l+2\sin\rho_l\sin\rho_r\cos\theta}}. \tag{31}$$

The coefficients related to Sarma's disturbance force vector $\boldsymbol{w}'$ could be expressed in similar equations. Replacing all the arguments related to '$\boldsymbol{w}$' in Eqs. (27)–(31) with $\boldsymbol{w}'$, we obtain all necessary relationships for $\boldsymbol{w}'$.

(3) For γ_l and γ_r, we have [refer to Eqs. (10) and (11)]

$$\left.\begin{aligned}\cos\gamma_l &= -\boldsymbol{t}_l\cdot\boldsymbol{j} = a_m\sec\rho_l\\ \cos\gamma_r &= -\boldsymbol{t}_r\cdot\boldsymbol{j} = a_m\sec\rho_r\end{aligned}\right\} \tag{32}$$

3. Generalized formulations

3.1. Solutions for the 'factor of safety approach'

(1) *The equation for solving the factor of safety*. Assume that the wedge block is in a limiting equilibrium state and shear failure develops on the left and right planes. The wedge moves in a direction of $\boldsymbol{m}$. The generalized solution is obtained by projecting all the forces applied on the wedge on an axis that is perpendicular to both the left and right 'combined friction force' vectors $\boldsymbol{p}_l$ and $\boldsymbol{p}_r$. This enables the elimination of the unknown $\boldsymbol{P}_l$ and $\boldsymbol{P}_r$, leaving only one unknown, the factor of safety F, involved in the force equilibrium equation. The direction of this axis can be represented by vector $\boldsymbol{Q}$, the cross product of $\boldsymbol{p}_l$ and $\boldsymbol{p}_r$, which are found in Eqs. (13) and (14).

$$\begin{aligned}\boldsymbol{Q} = \boldsymbol{p}_l\times\boldsymbol{p}_r = &-\frac{\sin\phi_{el}\cos(\rho_r-\phi_{er})}{\cos\rho_l\cos\rho_r}\boldsymbol{m}\times\boldsymbol{n}_r\\ &-\frac{\sin\phi_{er}\cos(\rho_l-\phi_{el})}{\cos\rho_l\cos\rho_r}\boldsymbol{n}_l\times\boldsymbol{m}\\ &+\frac{\cos(\rho_l-\phi_{el})\cos(\rho_r-\phi_{er})}{\cos\rho_l\cos\rho_r}\boldsymbol{n}_l\times\boldsymbol{n}_r.\end{aligned} \tag{33}$$

By virtue of Eqs. (10), (11) and (28)–(31) the projections of cohesion forces $\boldsymbol{C}_{el}$, $\boldsymbol{C}_{er}$ and external weight $\boldsymbol{W}$ on $\boldsymbol{Q}$ are expressed respectively as follows:

$$\begin{aligned}\boldsymbol{Q}\cdot\boldsymbol{C}_{el} &= c_{el}A_l\boldsymbol{Q}\cdot\boldsymbol{t}_l\\ &= \left[\frac{\sin\phi_{el}\cos(\rho_r-\phi_{er})}{\cos\rho_l\cos\rho_r}\tan\rho_l\right.\\ &\quad\left.-\frac{\cos(\rho_l-\phi_{el})\cos(\rho_r-\phi_{er})}{\cos\rho_l\cos\rho_r}\sec\rho_l\right]c_{el}A_l\boldsymbol{m}\cdot\boldsymbol{j}/\Delta\\ &= -\cos\phi_{el}\cos(\rho_r-\phi_{er})\\ &\quad\times c_{el}A_l\sec\rho_l\sec\rho_r\boldsymbol{m}\cdot\boldsymbol{j}/\Delta,\end{aligned} \tag{34}$$

$$\begin{aligned}\boldsymbol{Q}\cdot\boldsymbol{C}_{er} &= c_{er}A_r\boldsymbol{Q}\cdot\boldsymbol{t}_r\\ &= \left[\frac{\sin\phi_{er}\cos(\rho_l-\phi_{el})}{\cos\rho_l\cos\rho_r}\tan\rho_l\right.\\ &\quad\left.-\frac{\cos(\rho_r-\phi_{er})\cos(\rho_l-\phi_{el})}{\cos\rho_l\cos\rho_r}\sec\rho_r\right]c_{er}A_r\boldsymbol{m}\cdot\boldsymbol{j}/\Delta\\ &= -\cos\phi_{er}\cos(\rho_l-\phi_{el})\\ &\quad\times c_{er}A_r\sec\rho_l\sec\rho_r\boldsymbol{m}\cdot\boldsymbol{j}/\Delta\end{aligned} \tag{35}$$

$$\begin{aligned}\boldsymbol{Q}\cdot\boldsymbol{W} &= W\boldsymbol{Q}\cdot\boldsymbol{w}\\ &= [\sin\phi_{el}\cos(\rho_r-\phi_{er})b_w+\cos(\rho_l-\phi_{el})\sin\phi_{er}c_w\\ &\quad+a_w w\cos(\rho_l-\phi_{el})\cos(\rho_r-\phi_{er})]\\ &\quad\times\sec\rho_l\sec\rho_r W\boldsymbol{m}\cdot\boldsymbol{j}/\Delta,\end{aligned} \tag{36}$$

where A_l and A_r are areas of the left and right failure planes, respectively.

The force equilibrium condition is

$$\boldsymbol{Q}\cdot\boldsymbol{C}_{el}+\boldsymbol{Q}\cdot\boldsymbol{C}_{er}+\boldsymbol{Q}\cdot\boldsymbol{W}=0 \tag{37}$$

which leads to

$$\begin{aligned}\Omega(\rho_l,\rho_r,F) = &-\cos\phi_{el}\cos(\rho_r-\phi_{er})c_{el}A_l\\ &-\cos\phi_{er}\cos(\rho_l-\phi_{el})c_{er}A_r\\ &+[\sin\phi_{el}\cos(\rho_r-\phi_{er})b_w\\ &+\cos(\rho_l-\phi_{el})\sin\phi_{er}c_w\\ &+a_w\cos(\rho_l-\phi_{el})\cos(\rho_r-\phi_{er})]W\\ =&\,0.\end{aligned} \tag{38}$$

Eq. (38) is the governing equation of the generalized method and involves an unknown variable F that is included in the variables with subscripts 'e'. Once a set of ρ_l and ρ_r is input into Eq. (38), F can be obtained by iterations. It has been found that the Newton–Raphson method in most cases allows very rapid convergence in the numerical procedures.

(2) *Solutions for the normal forces*. Once the factor of safety is obtained, the normal forces $\boldsymbol{N}_l$ and $\boldsymbol{N}_r$ can be readily determined. A convenient way of obtaining $\boldsymbol{N}_l$ can be projecting all the forces on the axis that is perpendicular to $\boldsymbol{n}_r$ and $\boldsymbol{t}_r$, designated $\boldsymbol{U}$. Consequently the internal forces applying on the right plane do not appear in the projection, leaving only one unknown $\boldsymbol{N}_l$ to be obtained. $\boldsymbol{U}$ is represented by

$$\begin{aligned}\boldsymbol{U} &= \boldsymbol{t}_r\times\boldsymbol{n}_r = (-\boldsymbol{m}\sec\rho_r+\boldsymbol{n}_r\tan\rho_r)\times\boldsymbol{n}_r\\ &= -\boldsymbol{m}\times\boldsymbol{n}_r\sec\rho_r.\end{aligned} \tag{39}$$

Projections of $\boldsymbol{t}_l$, $\boldsymbol{n}_l$ and $\boldsymbol{w}$ on $\boldsymbol{U}$ are determined by the following equations, respectively:

$$\begin{aligned}\boldsymbol{U}\cdot\boldsymbol{t}_l &= (-\boldsymbol{m}\times\boldsymbol{n}_r\sec\rho_r)\cdot(-\boldsymbol{m}\sec\rho_l+\boldsymbol{n}_l\tan\rho_l)\\ &= \tan\rho_l\sec\rho_r\boldsymbol{m}\cdot\boldsymbol{j}/\Delta,\end{aligned} \tag{40}$$

$$\boldsymbol{U}\cdot\boldsymbol{n}_l = \sec\rho_r\boldsymbol{m}\cdot\boldsymbol{j}/\Delta, \tag{41}$$

$$\begin{aligned}\boldsymbol{U}\cdot\boldsymbol{w} &= (-\boldsymbol{m}\times\boldsymbol{n}_r\sec\rho_r)\cdot(a_w\boldsymbol{m}+b_w\boldsymbol{n}_l+c_w\boldsymbol{n}_r)\\ &= b_w\sec\rho_r\boldsymbol{m}\cdot\boldsymbol{j}/\Delta.\end{aligned} \tag{42}$$

The condition that

$$\boldsymbol{U}\cdot\boldsymbol{n}_{\mathrm{l}}N_{\mathrm{l}}+(c_{\mathrm{el}}A_{\mathrm{l}}+N_{\mathrm{l}}\tan\phi_{\mathrm{el}})\boldsymbol{U}\cdot\boldsymbol{t}_{\mathrm{l}}+\boldsymbol{U}\cdot\boldsymbol{w}W=0 \quad (43)$$

gives

$$N_{\mathrm{l}}=-\frac{c_{\mathrm{el}}A_{\mathrm{l}}\tan\rho_{\mathrm{l}}+b_wW}{1+\tan\rho_{\mathrm{l}}\tan\phi_{\mathrm{el}}}. \quad (44)$$

A similar derivation gives

$$N_{\mathrm{r}}=-\frac{c_{\mathrm{er}}A_{\mathrm{r}}\tan\rho_{\mathrm{r}}+c_wW}{1+\tan\rho_{\mathrm{r}}\tan\phi_{\mathrm{er}}}. \quad (45)$$

(3) *The condition of physical admissibility*. The input of ρ_{l} and ρ_{r} are not arbitrary, but subject to some kinematic conditions. In other words, the wedge may not be able to dilate in the specified values of ρ_{l} and ρ_{r} on some occasions. The admissibility condition may be stated such that a_m defined by Eq. (26) must have a real root, i.e.

$$\sin^2\theta-\sin^2\rho_{\mathrm{r}}-\sin^2\rho_{\mathrm{l}}+2\sin\rho_{\mathrm{l}}\sin\rho_{\mathrm{r}}\cos\theta\geqslant 0. \quad (46)$$

If a set of ρ_{l} and ρ_{r} violates the requirement for physical admissibility, it will be rejected. The factors of safety may be bounded by a series of solutions related to the input of ρ_{l} and ρ_{r} that satisfies the equality condition of Eq. (46). Example 3 in Section 3.3 gives further explanation.

(4) *Solutions for the case of tension on one plane*. If the normal force on a plane calculated from either Eq. (44) or Eq. (45) is negative, tension would develop on one plane and the wedge would separate from that plane first, followed by a slip along the steepest descendent direction of the other plane. Solutions related to this case have been discussed by Hoek and Bray [1]. In the generalized solution, a procedure of checking $\boldsymbol{N}_{\mathrm{l}}$ or $\boldsymbol{N}_{\mathrm{r}}$ associated with all possible input of ρ_{l} and ρ_{r} is performed. Only when all possible $\boldsymbol{N}_{\mathrm{l}}$ or $\boldsymbol{N}_{\mathrm{r}}$ values are negative will the wedged be analyzed on the 'tension failure' basis, as shown in Example 2 of Section 3.3.

In the case of $\boldsymbol{N}_{\mathrm{r}}\leqslant 0$ for all possible ρ_{l} and ρ_{r}, $\boldsymbol{t}_{\mathrm{l}}$, $\boldsymbol{n}_{\mathrm{l}}$ and $\boldsymbol{w}$ lie on the same plane. The factor of safety is determined by

$$F=\frac{c_{\mathrm{l}}A_{\mathrm{l}}+W\cos\psi\tan\phi_{\mathrm{l}}}{W\sin\psi}, \quad (47)$$

where ψ is the angle between $\boldsymbol{n}_{\mathrm{l}}$ and $\boldsymbol{w}$. Similar derivation can find the factor of safety for the case of $\boldsymbol{N}_{\mathrm{l}}\leqslant 0$.

3.2. Solutions for the 'critical acceleration approach'

In the critical acceleration approach, the strength parameters are not reduced, which means subscripts 'e' involved in all equations in Section 3.1 no longer exist. As a substitution, the coefficient of critical acceleration η is added, making an equation equivalent to Eq. (37) as

$$\boldsymbol{Q}\cdot\boldsymbol{C}_{\mathrm{l}}+\boldsymbol{Q}\cdot\boldsymbol{C}_{\mathrm{r}}+\boldsymbol{Q}\cdot\boldsymbol{W}+\boldsymbol{Q}\cdot\eta\boldsymbol{W}'=0 \quad (48)$$

from which we have

$$\eta=\frac{\cos\phi_{\mathrm{l}}\cos(\rho_{\mathrm{r}}-\phi_{\mathrm{r}})c_{\mathrm{l}}A_{\mathrm{l}}+\cos\phi_{\mathrm{r}}\cos(\rho_{\mathrm{l}}-\phi_{\mathrm{l}})c_{\mathrm{r}}A_{\mathrm{r}}}{[\sin\phi_{\mathrm{l}}\cos(\rho_{\mathrm{r}}-\phi_{\mathrm{r}})b_{w'}+\cos(\rho_{\mathrm{l}}-\phi_{\mathrm{l}})\sin\phi_{\mathrm{r}}c_{w'}+a_{w'}w\cos(\rho_{\mathrm{l}}-\phi_{\mathrm{l}})\cos(\rho_{\mathrm{r}}-\phi_{\mathrm{r}})]W'}-\frac{[\sin\phi_{\mathrm{l}}\cos(\rho_{\mathrm{r}}-\phi_{\mathrm{r}})b_w+\cos(\rho_{\mathrm{l}}-\phi_{\mathrm{l}})\sin\phi_{\mathrm{r}}c_w+a_ww\cos(\rho_{\mathrm{l}}-\phi_{\mathrm{l}})\cos(\rho_{\mathrm{r}}-\phi_{\mathrm{r}})]W}{[\sin\phi_{\mathrm{l}}\cos(\rho_{\mathrm{r}}-\phi_{\mathrm{r}})b_{w'}+\cos(\rho_{\mathrm{l}}-\phi_{\mathrm{l}})\sin\phi_{\mathrm{r}}c_{w'}+a_{w'}w\cos(\rho_{\mathrm{l}}-\phi_{\mathrm{l}})\cos(\rho_{\mathrm{r}}-\phi_{\mathrm{r}})]W'}. \quad (49)$$

The arguments related to the determination of normal forces, the requirements for physical admissibility and check of tension on the failure planes described in Section 3.1 are similar and not listed here.

3.3. Illustrative examples

A computer program has been developed to implement the numerical procedures described in this section.[2] To make the output more illustrative, the values of ρ_{l} and ρ_{r} that satisfy Eq. (38) are expressed by ρ'_{l} and ρ'_{r} with the definition:

$$\left.\begin{aligned}\tan\rho_{\mathrm{l}}&=\frac{\tan\rho'_{\mathrm{l}}}{F}\\ \tan\rho_{\mathrm{r}}&=\frac{\tan\rho'_{\mathrm{r}}}{F}\end{aligned}\right\} \quad (50)$$

ρ'_{l} and ρ'_{r} are called unreduced values of ρ_{l} and ρ_{r} and will be compared with the unreduced values ϕ_{l} and ϕ_{r}, as will be shown in the subsequent examples.

Example 1. This problem is related to a typical wedge with the geometry and geotechnical properties shown in Table 2.

Values of the factors of safety associated with various inputs of ρ_{l} and ρ_{r} were obtained by solving Eq. (38). All solutions have positive normal forces N_{l} and N_{r}, obtained from Eqs. (44) and (45). Fig. 7(a) shows the contours of F versus ρ'_{l} and ρ'_{r}.

From these contours, one finds a maximum value of $F=1.521$ that is associated with $\rho'_{\mathrm{l}}=\phi_{\mathrm{l}}=20^\circ$ and $\rho'_{\mathrm{r}}=\phi_{\mathrm{r}}=30^\circ$ (or $\rho_{\mathrm{l}}=\phi_{\mathrm{el}}=13.46^\circ$ and $\rho_{\mathrm{r}}=\phi_{\mathrm{er}}=20.79^\circ$). The traditional method associated with $\rho'_{\mathrm{l}}=0$ and $\rho'_{\mathrm{r}}=0$ gives $F=1.411$. Fig. 7(b) gives the 'equal η contours' for the 'disturbance force approach' based on Eq. (49).

[2] The source programs and data files of all the examples described in this paper can be found at the web site: www.geoeng.iwhr.com/geoeng/download.htm.

Table 2
Parameters for Test problem 1

Surface	Dip direction	Dip angle	Friction angle	Cohesion (9.8 kPa)
Left	105°	45°	20°	5
Right	235°	70°	30°	5
Crest	195°	12°		
Slope	185°	65°		

Note: Height = 100 m, and unit weight = 2.6×9.8 kN/m^3.

Table 3
Parameters for Test problem 2

Surface	Dip direction	Dip angle	Friction angle	Cohesion (kPa)
Left	195°	60°	35	29.4
Right	235°	70°	30	29.4
Crest	195°	12°		
Slope	185°	65°		

Note: Height = 100 m and unit weight = 2.6×9.8 kN/m^3.

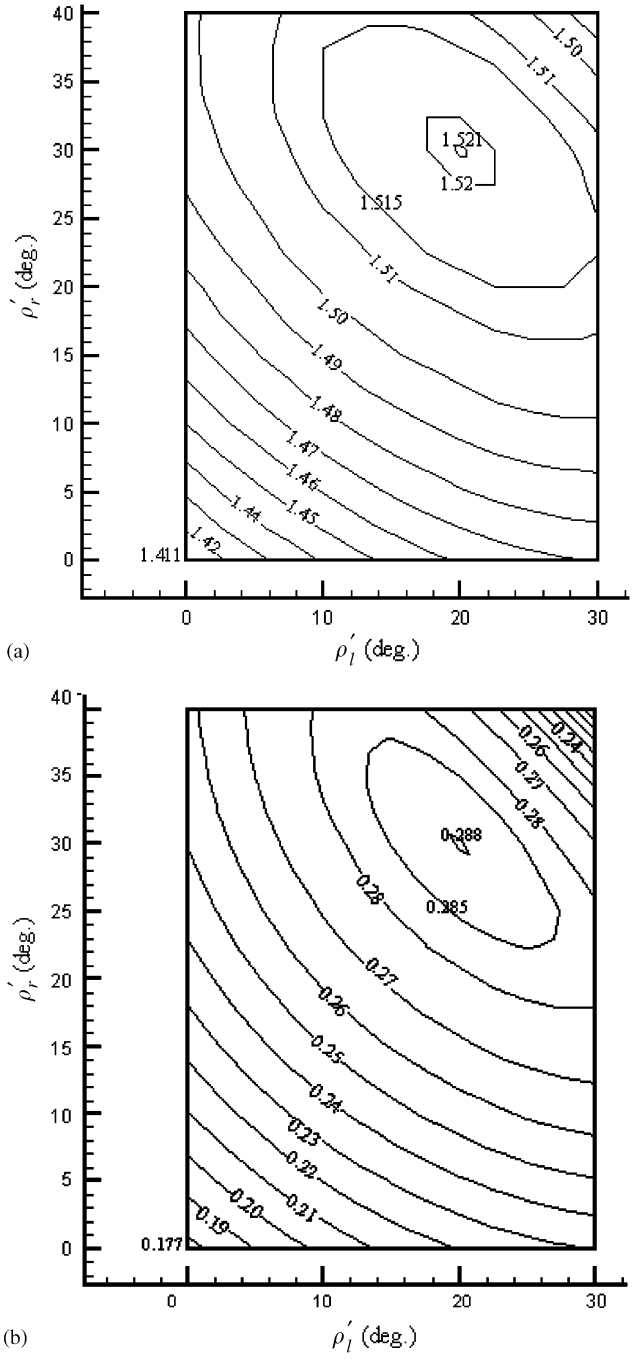

Fig. 7. Solutions of Example 1 associated with various ρ_l' and ρ_r': (a) contours of equal F and (b) contours of equal η.

Again it confirms that at $\rho_l = \phi_l$ and $\rho_r = \phi_r$, η reached a maximum of 0.288.

Example 2. This problem is purposely designed to have steep dip angles and relatively large friction angles related to the two failure planes, as shown in Table 3. Some unusual behavior is expected to occur.

Fig. 8 gives the calculated details associated with various ρ_l' and ρ_r'. It can be found that a majority of solutions, including those given by the traditional method, are related to negative values of N_l or N_r. However, there is still an area that does provide reasonable values of F associated with positive normal forces N_l and N_r, which are ranged between 0.975 and 0.80, as shown in Fig. 8. Within the framework of the generalized method, this problem is still considered a typical wedge shear failure rather than that of 'tension plane' case.

Example 3. This problem is taken from Case No. 3 of the example of the Three Gorges Project ship lock slope that will be discussed in more detail in Section 5. The input parameters are shown in Table 4. The large value of θ, the angle between the normals of the two failure planes, makes Eq. (46) unsatisfied at some values of ρ_l and ρ_r. Fig. 9 shows the area that Eq. (46) fails to apply, and the factor of safety at $\rho_l = \phi_{el}$ and $\rho_r = \phi_{er}$ is not obtainable. The physically admissible solutions are bounded by an equal F contour of $F = 1.40$, more thorough search gave a maximum value of $F = 1.419$.

4. Theoretical aspects

4.1. Demonstration of the 'Principle of maximum'

From the results of the examples shown in the Introduction and Section 3.3, we found that a maximum factor of safety or coefficient of critical acceleration exists when the wedge dilates at friction angles to the failure planes. With the governing equation (38) or (49), it is possible to give a formal demonstration.

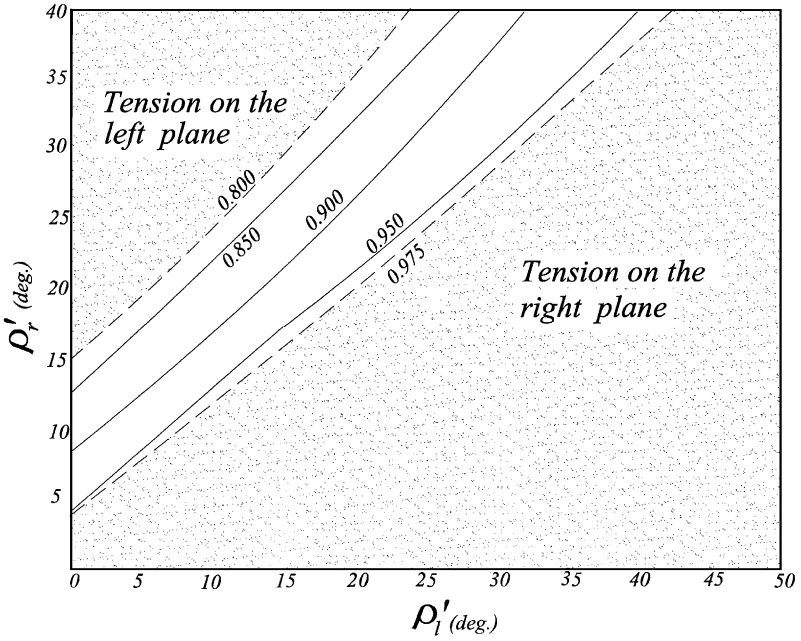

Fig. 8. Contours of factors of safety for Test problem 2 and the areas of 'tension plane'.

Table 4
Parameters for Test problem 3

Surface	Dip direction	Dip angle	Friction angle	Cohesion
Left	345°	60°	31°	0
Right	76°	70°	31°	0
Crest	201°	0°		
Slope	201°	90°		

Note: Height = 100 m, unit weight = 2.7×9.8 kN/m^3 and $r_u = 0.1$.

(1) *The 'factor of safety approach'*. The statement for the 'factor of safety approach' is as follows:

Among all kinematically admissible sets of ρ_l *and* ρ_r, *the one associated with* $\rho_l = \phi_{el}$ *and* $\rho_r = \phi_{er}$ *makes* F, *determined by Eq.* (38), *a maximum*.

Suppose there is an increment in $\Delta\rho_l$ that results in an increment in ΔF. To ensure that Eq. (38) still applies, the following equation must be satisfied:

$$\frac{\partial \Omega}{\partial \rho_l}\Delta\rho_l + \frac{\partial \Omega}{\partial F}\Delta F = 0 \tag{51}$$

or

$$\frac{\partial \Omega}{\partial \rho_l} + \frac{\partial \Omega}{\partial F}\frac{\partial F}{\partial \rho_l} = 0. \tag{52}$$

Therefore, the necessary condition that makes $\partial F/\partial\rho_l = 0$ is $\partial\Omega/\partial\rho_l = 0$. The same condition applies to the argument for ρ_r. We then go on demonstrating the following statement:

Among all kinematically admissible sets of ρ_l *and* ρ_r, *the one associated with* $\rho_l = \phi_{el}$ *and* $\rho_r = \phi_{er}$ *makes* $\partial\Omega/\partial\rho_l = 0$ and $\partial\Omega/\partial\rho_r = 0$.

Substituting Eqs. (28) and (29) into Eq. (38) We have

$$\begin{aligned}\Omega(\rho_l, \rho_r, F) = & -\cos\phi_{el}\cos(\rho_r - \phi_{er})c_{el}A_l \\ & -\cos\phi_{er}\cos(\rho_l - \phi_{el})c_{er}A_r \\ & +(\boldsymbol{w}\cdot\boldsymbol{n}_l - \boldsymbol{w}\cdot\boldsymbol{n}_r\cos\theta)\sin\phi_{el} \\ & \times\cos(\rho_r - \phi_{er})\,\mathrm{cosec}^2\,\theta W \\ & +(\boldsymbol{w}\cdot\boldsymbol{n}_r - \boldsymbol{w}\cdot\boldsymbol{n}_l\cos\theta)\sin\phi_{er}\cos(\rho_l - \phi_{el}) \\ & \times\mathrm{cosec}^2\,\theta W + a_w[(\sin\rho_r\cos\theta - \sin\rho_l) \\ & \times\sin\phi_{er}\cos(\rho_r - \phi_{er}) \\ & +(\sin\rho_l\cos\theta - \sin\rho_r)\sin\phi_{er}\cos(\rho_l - \phi_{el}) \\ & +\cos(\rho_l - \phi_{el})\cos(\rho_r - \phi_{er}) \\ & \times\sin^2\theta]\,\mathrm{cosec}^2\,\theta W = 0.\end{aligned} \tag{53}$$

It is obvious that the previous four terms on the right-hand side of Eq. (53) have their first-order partial derivatives for ρ_l and ρ_r respectively set to zero at $\rho_l = \phi_{el}$ and $\rho_r = \phi_{er}$. We now concentrate on demonstrating that at $\rho_l = \phi_{el}$ and $\rho_r = \phi_{er}$, the following equations apply:

$$\begin{aligned}S_l = \frac{\partial}{\partial\rho_l}\{a_w[&(\sin\rho_r\cos\theta - \sin\rho_l)\sin\phi_{el}\cos(\rho_r - \phi_{er}) \\ &+(\sin\rho_l\cos\theta - \sin\rho_r)\sin\phi_{er}\cos(\rho_l - \phi_{el}) \\ &+\cos(\rho_l - \phi_{el})\cos(\rho_r - \phi_{er})\sin^2\theta]\} = 0\end{aligned} \tag{54}$$

and

$$\begin{aligned}S_r = \frac{\partial}{\partial\rho_r}\{a_w[&(\sin\rho_r\cos\theta - \sin\rho_l)\sin\phi_{el}\cos(\rho_r - \phi_{er}) \\ &+(\sin\rho_l\cos\theta - \sin\rho_r)\sin\phi_{er}\cos(\rho_l - \phi_{el}) \\ &+\cos(\rho_l - \phi_{el})\cos(\rho_r - \phi_{er})\sin^2\theta]\} = 0.\end{aligned} \tag{55}$$

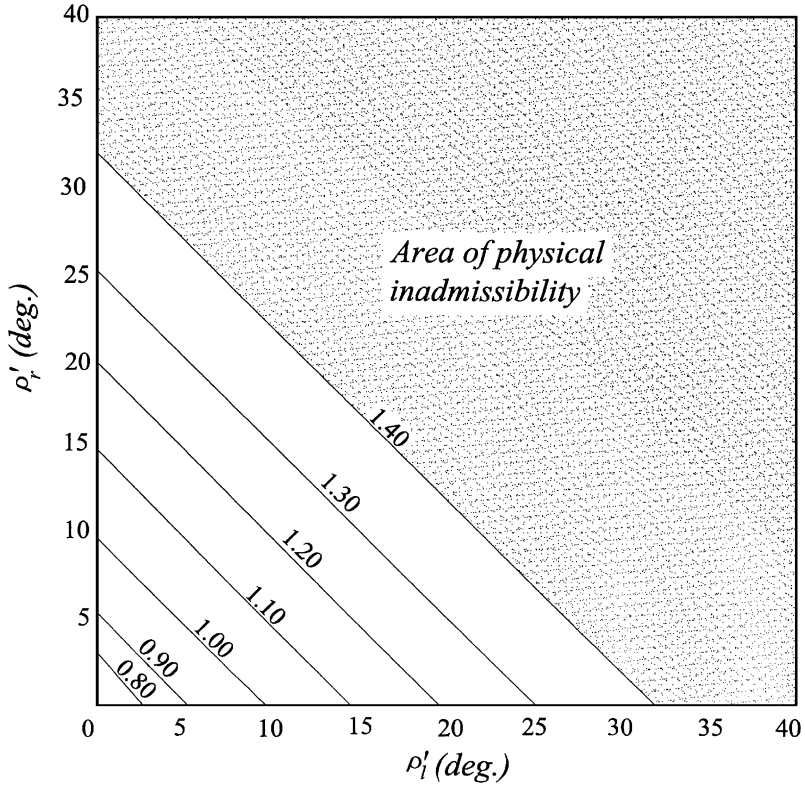

Fig. 9. Contours of factors of safety for Test problem 3 and the area that violates the condition of physical admissibility.

S_l can be separated by two parts.

$$S_l = A_1 + A_2, \tag{56}$$

where:

$$\begin{aligned} A_1 = \frac{\partial a_w}{\partial \rho_l}[&(\sin\rho_r\cos\theta - \sin\rho_l)\sin\phi_{el}\cos(\rho_r - \phi_{er}) \\ &+ (\sin\rho_l\cos\theta - \sin\rho_r)\sin\phi_{er}\cos(\rho_l - \phi_{el}) \\ &+ \cos(\rho_l - \phi_{el})\cos(\rho_r - \phi_{er})\sin^2\theta], \end{aligned} \tag{57}$$

$$\begin{aligned} A_2 = a_w[&-\cos\rho_l\sin\phi_{el}\cos(\rho_r - \phi_{er}) + \cos\rho_l\cos\theta\sin\phi_{er} \\ &\times\cos(\rho_l - \phi_{el}) - (\sin\rho_l\cos\theta - \sin\rho_r) \\ &\times\sin\phi_{er}\sin(\rho_l - \phi_{el}) - \sin(\rho_l - \phi_{el}) \\ &\times\cos(\rho_r - \phi_{er})\sin^2\theta]. \end{aligned} \tag{58}$$

We introduce the following basic relationships from Eq. (26) and Eq. (31):

$$\frac{\partial a_m}{\partial \rho_l} = \frac{1}{a_m}\operatorname{cosec}^2\theta(\cos\rho_l\sin\rho_r\cos\theta - \sin\rho_l\cos\rho_l), \tag{59}$$

$$\begin{aligned} \frac{\partial}{\partial\rho_l}\left(\frac{1}{a_m}\right) = &-\frac{1}{a_m^3}\operatorname{cosec}^2\theta \\ &\times(\cos\rho_l\sin\rho_r\cos\theta - \sin\rho_l\cos\rho_l), \end{aligned} \tag{60}$$

$$\begin{aligned} \frac{\partial a_w}{\partial \rho_l} = &-\boldsymbol{w}\cdot\boldsymbol{j}\frac{1}{a_m^3}\operatorname{cosec}^2\theta \\ &\times(\cos\rho_l\sin\rho_r\cos\theta - \sin\rho_l\cos\rho_l). \end{aligned} \tag{61}$$

By substituting Eqs. (59) and (61) into Eqs. (57) and (58), one obtains

$$\begin{aligned} A_1 = &-\boldsymbol{w}\cdot\boldsymbol{j}\frac{1}{a_m^3}(\cos\rho_l\sin\rho_r\cos\theta - \sin\rho_l\cos\rho_l) \\ &\times[(\sin\rho_r\cos\theta - \sin\rho_l)\sin\phi_{el}\cos(\rho_r - \phi_{er}) \\ &+ (\sin\rho_l\cos\theta - \sin\rho_r)\sin\phi_{er}\cos(\rho_l - \phi_{el}) \\ &+ \cos(\rho_l - \phi_{el})\cos(\rho_r - \phi_{er})\sin^2\theta]\operatorname{cosec}^2\theta \end{aligned} \tag{62}$$

and

$$\begin{aligned} A_2 = &\frac{\boldsymbol{w}\cdot\boldsymbol{j}}{a_m^3}(\sin^2\theta - \sin^2\rho_r - \sin^2\rho_l + 2\sin\rho_l\sin\rho_r\cos\theta) \\ &\times[-\cos\rho_l\sin\phi_{el}\cos(\rho_r - \phi_{er}) \\ &+ \cos\rho_l\cos\theta\sin\phi_{er}\cos(\rho_l - \phi_{el}) - (\sin\rho_l\cos\theta \\ &- \sin\rho_r)\sin\phi_{er}\sin(\rho_l - \phi_{el}) \\ &- \sin(\rho_l - \phi_{el})\cos(\rho_r - \phi_{er})\sin^2\theta]\operatorname{cosec}^2\theta. \end{aligned} \tag{63}$$

It is not difficult to find that for $\rho_l = \phi_{el}$ and $\rho_r = \phi_{er}$, the reduced expressions of Eqs. (62) and (63) make Eq. (54) apply. A similar derivation will prove Eq. (55).

A complete demonstration requires the sufficient conditions $\partial^2 F/\partial\rho_l^2 < 0$ and $\partial^2 F/\partial\rho_r^2 < 0$ to be satisfied

at $\rho_l = \phi_{el}$ and $\rho_r = \phi_{er}$. However, as in many areas related to the determinations of extremes (e.g. the finite element formulations based on the 'principle of minimum potential energy'), this statement is not demonstrated on an analytical basis but justified through practical applications. The test problems described in this paper and many subsequent applications follow this rule.

(2) *The* '*critical acceleration approach*'. The statement of the 'principle of maximum' for the 'critical acceleration approach' is as follows:

Among all kinematically admissible sets of ρ_l *and* ρ_r, *the one associated with* $\rho_l = \phi_l$ *and* $\rho_r = \phi_r$ *makes* $\partial\eta/\partial\rho_l = 0$ and $\partial\eta/\partial\rho_r = 0$, where η is determined by Eq. (49).

Eq. (49) can be written as

$$\eta = \frac{B_2}{B_1} + \frac{B_3}{B_1}, \tag{64}$$

where

$$B_1 = [\sin\phi_l \cos(\rho_r - \phi_r) b_{w'} + \cos(\rho_l - \phi_l)\sin\phi_r \cdot c_{w'} + a_{w'} w \cos(\rho_l - \phi_l)\cos(\rho_r - \phi_r)]W',$$

$$B_2 = \cos\phi_l \cos(\rho_r - \phi_r) c_l A_l + \cos\phi_r \cos(\rho_l - \phi_l) c_r A_r, \tag{65}$$

$$B_3 = [\sin\phi_l \cos(\rho_r - \phi_r) b_w + \cos(\rho_l - \phi_l)\sin\phi_r \cdot c_w + a_w w \cos(\rho_l - \phi_l)\cos(\rho_r - \phi_r)]W. \tag{66}$$

We have

$$\frac{\partial\eta}{\partial\rho_l} = \frac{1}{B_1}\frac{\partial B_2}{\partial\rho_l} - \frac{1}{B_1^2}\frac{\partial B_1}{\partial\rho_l}B_2 + \frac{1}{B_1}\frac{\partial B_3}{\partial\rho_l} - \frac{1}{B_1^2}\frac{\partial B_1}{\partial\rho_l}B_3. \tag{67}$$

By procedures almost identical to those described in the previous paragraph, it is possible to demonstrate that at $\rho_l = \phi_l$ and $\rho_r = \phi_r$,

$$\frac{\partial B_1}{\partial\rho_l} = 0, \quad \frac{\partial B_2}{\partial\rho_l} = 0, \quad \text{and} \quad \frac{\partial B_3}{\partial\rho_l} = 0 \tag{68}$$

which leads to

$$\frac{\partial\eta}{\partial\rho_l} = 0. \tag{69}$$

Similar arguments will demonstrate that at $\rho_l = \phi_l$ and $\rho_r = \phi_r$:

$$\frac{\partial\eta}{\partial\rho_r} = 0. \tag{70}$$

4.2. Reducing the generalized solutions to the special cases

In the illustrative example of Introduction, two special cases lead to the solutions to F being equal to 0.727 and 1.002, respectively. The first case, referred here as 'conventional' or 'traditional' method, assumes that γ_l and γ_r are zero. This case actually means non-dilative behavior of the material (ρ_l and ρ_r are zero). The second case starts from plastic velocity of the wedge that dilates at values of friction angles to the two failure planes. The work-energy balance equation involved in the Upper Bound Theorem permits a solution, which has been demonstrated to be associated with the maximum possible factor of safety of the wedge.

It has been found that the generalized solution is reducible to the two cases. A formal demonstration is given in the appendix.

4.3. Discussions on the theoretical implication of the generalized solution

Suppose that a set of internal force balances the external loads:

$$\boldsymbol{C}_l + \boldsymbol{C}_r + \boldsymbol{P}_l + \boldsymbol{P}_r + \boldsymbol{W} + \eta\boldsymbol{W}' = 0. \tag{71}$$

According to the demonstration in Section 4.1, if $\rho_l < \phi_l$ and $\rho_r < \phi_r$, further loading related to a positive $\Delta\eta$ is possible to transfer the equilibrium to a new state that satisfies

$$\boldsymbol{C}_l + \Delta\boldsymbol{C}_l + \boldsymbol{C}_r + \Delta\boldsymbol{C}_r + \boldsymbol{P}_l + \Delta\boldsymbol{P}_l + \boldsymbol{P}_r + \Delta\boldsymbol{P}_r + \boldsymbol{W} + (\eta + \Delta\eta)\boldsymbol{W}' = 0. \tag{72}$$

The plastic velocity developed by the increment of external load $\Delta\eta\,\boldsymbol{W}'$ is $\boldsymbol{V}$. Then [Eq. (72)-Eq. (71)] $\times\,\boldsymbol{V}$ gives

$$-(\Delta\boldsymbol{C}_l \cdot \boldsymbol{V} + \Delta\boldsymbol{C}_r \cdot \boldsymbol{V} + \Delta\boldsymbol{P}_l \cdot \boldsymbol{V} + \Delta\boldsymbol{P}_r \cdot \boldsymbol{V}) = \Delta\eta\,\boldsymbol{W}' \cdot \boldsymbol{V}. \tag{73}$$

The left-hand side of Eq. (73) is the plastic energy done by the stress increment and represented by $\int_{A_l} \mathrm{d}\sigma_{ij}\,\dot{\varepsilon}\,\mathrm{d}A_l + \int_{A_r} \mathrm{d}\sigma_{ij}\,\dot{\varepsilon}\,\mathrm{d}A_r$, where $\mathrm{d}\sigma_{ij}$ and $\dot{\varepsilon}$ denote the stress increment and the plastic velocity incurred by the stress increment, respectively. According to Drucker's Postulate, this term should be non-negative if the material is stable. It follows that $\Delta\eta$ is non-negative.

We now come to the conclusion that the 'principle of maximum' is in fact another way to describe Drucker's Postulate. However, the positive value of $\Delta\eta$ is confirmed by the rigorous mathematical demonstrations. The generalized solution thus presents a support to Drucker's Postulate under a special condition—the wedge failure.

It has been demonstrated that no further loading would be possible at $\rho_l = \phi_l$ and $\rho_r = \phi_r$. The generalized solution therefore presents another support to the Mohr–Coulomb's associative flow law under the special condition—the wedge failure.

We know that neither Drucker's Postulate nor the 'principle of maximum' is a fully proven fundamental law of nature. The theoretical implication of the generalized solutions described in this paper may be interpreted in the following several alternative ways.

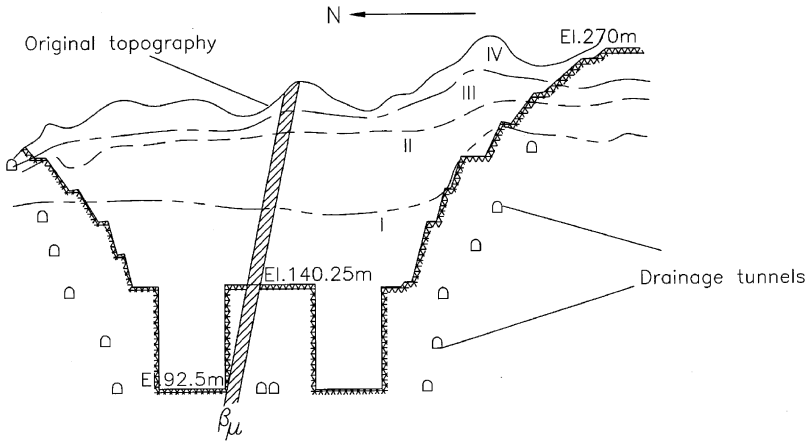

Fig. 10. A typical cross section of the ship lock slope of the Three Gorges Project. *Legend*: IV, III, II, I refer to the completely, heavily, slightly weathered and intact rock mass, respectively. β_μ is the pegmatitic dikes.

(1) When a wedge is under loading, it would dilate as much as possible to accommodate the external load. The maximum resistance occurs when it dilates at values of friction angles to its respective failure planes.
(2) Dilation is a material behavior rather than a mechanical condition. Therefore, in addition to the conventional shear strength test, the dilation angle of the material upon failure should be measured by field and laboratory tests and treated as input in the generalized solution.
(3) As a controversial understanding, one may believe that a wedge would fail in a stress mode that provides the least resistance. Therefore, the traditional method is the only acceptable solution. Another argument may be that the traditional method relates to incipient failure, which may be transferred to imminent failure when the upper bound solution applies.

Alternative (1) gives the upper bound solution to the factor of safety. Alternative (3) normally gives the smallest factor of safety, although formal demonstration is not yet available. Alternative (2) gives an intermediate value of F.

Obviously, this is not only an issue of theory, but also a problem of practice and observation for the future. Performing physical model tests, preferably centrifuge tests, may be an approach to better understanding to these issues.

5. Applications

In order to understand the impact of the generalized solution on our routine design procedures, the author reviewed the wedge stability analysis results for the ship lock slope at the Three Gorges Project. This navigation facility contains two routes, each consisting of five levels of locks. A typical cross section of the ship lock is shown in Fig. 10, from which one may find that the locks have vertical side-walls, susceptible to wedge failure. Fig. 11 shows a typical wedge identified and reinforced by the designers. The axis of the ship lock line strikes at 111°. The dip directions of the left and right walls are 201° and 21°, respectively.[3] The geology of the rock mass consists of amphibole granite (Pre-Sinian Period) with four dominating sets of joints dipping at 50°–75°, which present wedge failure potentials. Pegmatitic dikes are commonly encountered, which may also contribute to wedge failures. A total of 40 long and persistent faults were discovered during excavation. These discontinuities provide multiple chances to create potentially unstable wedges. The geologists identified more than 200 potential wedges and investigated the stability for each one. Prestressed cables were installed if the wedge block was considered to be unstable.

The geologists recommended two alternatives for shear strength evaluations. The first one, called the 'pure friction approach', employs a unique friction angle of 31° for the two failure planes. The factor of safety using this parameter must be greater than unity. The second alternative, referred to as '$c-\phi$ approach', involves using a cohesion of 0.1 MPa with required factor of safety larger than 2.0. The investigation also includes two approaches for pore pressure input, i.e., $r_u = 0$ and 0.1, where r_u is the pore pressure coefficient.

The difference between the results of the conventional and upper bound methods is evaluated by the relative difference ξ defined as

$$\xi = \frac{F_u - F_c}{F_u}, \tag{74}$$

[3] In hydraulic engineering, people normally refer 'left' and 'right' by looking downstream of the river.

Fig. 11. A reinforced wedge in the ship lock (Three Gorges Project).

Table 5
Factors of safety of the Three Gorges Ship lock wedges, the '$c-\phi$ approach'

No.	Location	Failure planes	Dip direction	Dip angle	Height (m)	$r_u = 0$			$r_u = 0.10$		
						F_c	F_u	ξ (%)	F_c	F_u	ξ (%)
1	2-S-R	f_{1101} $f^{y3\text{-}84}_{(a)}$	91° 231°	70° 60°	34.8	1.932	2.077	7.0	1.644	1.813	9.3
2	2-S-L	f_{1101} $f^{y\text{-}71}_{(b9)z}$	94° 225°	70° 75°	28.4	2.654	2.854	7.0	2.266	2.488	8.9
3	3-N-R	f_{1008} $\beta_{\mu 1004}$	345° 130°	76° 80°	32.1	3.145	3.509	10.4	2.633	3.059	13.9
4	3-N-L	f_{1005} f^{3011}_{15}	244° 96°	70° 61°	24	4.293	4.428	3.0	3.859	4.008	3.7
5	4-N-L	f_{205} $f^{y\text{-}21}_{(A)4}$	280° 140°	60° 70°	14.9	4.604	4.707	2.2	4.055	4.172	2.8
6	4-S-R	$f^{y3\text{-}34}_{(c3)4}$	340°	70°	17.2	4.121	4.273	3.6	3.736	3.903	4.3
		$f^{y\text{-}35}_{(B3)4}$	120°	70°							

Note: (1) Unit weigh of rock = 2.7×9.8 kN/m^3. (2) In case No. 1, the symbol '2-S-R' means: Gate No. 2, the South Chamber, and the right side-wall. Similar explanations apply to the other cases. (3) The dip directions of the left and right side-walls are 201° and 21°, respectively.

where F_c and F_u are factors of safety associated with the conventional and upper bound methods, respectively.

Tables 5 and 6 present the factors of safety for six typical wedges evaluated by both the '$c-\phi$' and 'pure friction' approaches using the traditional and upper bound methods, respectively. All the cases are related to typical wedge failure with both traditional and upper bound solutions except Case 3 and $r_u = 0.1$ in Table 6, which fails to find F_u due to violation of the condition of physical admissibility. This case has been discussed in detail in Example 3 of Section 3.3.

The ξ values contained in the tables indicate that the deviation between the two approaches increases as the height of the wedge, pore pressure, or the friction angles of the material increases. Among them, the friction angle is the most prominent factor. Fig. 12 gives a sensitivity analysis by taking different cohesion for Case 3 ($r_u = 0$) in Table 5, from which we find that ξ varies from 10.4% to 39.6% as c changes from 0.1 MPa to zero.

The situation now encountered is quite similar to that when methods with fewer assumptions were developed

Table 6
Factors of safety of the Three Gorges ship lock wedges, the 'pure friction approach'

No.	Location	Failure planes	Dip direction	Dip angle	Height (m)	$r_u = 0$			$r_u = 0.10$		
						F_c	F_u	ξ (%)	F_c	F_u	ξ (%)
1	2-S-R	f_{1101} $f^{y3\text{-}84}_{(a)}$	91° 231°	70° 60°	34.8	0.913	1.191	23.3	0.625	0.988	36.7
2	2-S-L	f_{1101} $f^{y\text{-}71}_{(b9)z}$	94° 225°	70° 75°	28.4	0.921	1.397	34.1	0.522	1.173	55.5
3	3-N-R	f_{1008} $\beta_{\mu 1004}$	345° 130°	76° 80°	32.1	1.181	1.954	39.6	0.669	1.419[a]	52.9
4	3-N-L	f_{1005} f^{3011}_{15}	244° 96°	70° 61°	24	2.061	2.330	11.5	1.627	1.956	16.8
5	4-N-L	f_{205} $f^{y\text{-}21}_{(A)4}$	280° 140°	60° 70°	14.9	1.575	1.854	15.0	1.025	1.417	27.7
6	4-S-R	$f^{y3\text{-}34}_{(c3)4}$	340°	70°	17.2	1.362	1.770	23.1	0.978	1.495	34.6
		$f^{y\text{-}35}_{(B3)4}$	120°	70°							

Note: (1) Unit weight of rock $= 2.7 \times 9.8$ kN/m^3. (2) In case No. 1, the symbol '2-S-R' means: Gate No. 2, the South Chamber, and the right side-wall. Similar explanations apply to the other cases. (3) The dip directions of the left and right side-walls are 201° and 21°, respectively.

[a] This problem cannot find an upper bound solution as the condition of physical admissibility is violated. Details have been given in Test problem 3 of Section 3.3.

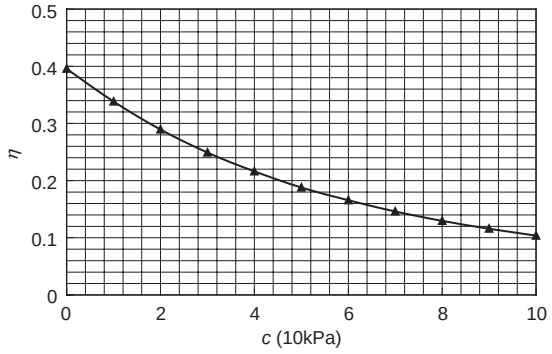

Fig. 12. Values of relative difference ξ associated with varying cohesion c for case 3 ($r_u = 0$) of Table 5.

in soil slope stability analysis, such as the Simplified Bishop's [13] and Morgenstern–Price [14] methods. It has been found that the traditional Swedish method (Fellenius, 1927) [15] normally underestimates the factor of safety by 10%. However, sometimes the deviation may be as large as 50% or more, if the values of the arc angle of the slip circle and the pore pressure are large [16–18]. In engineering practice, introducing more rigorous methods is normally accompanied by a more stringent requirement for allowable factor of safety. The Chinese Design Codes for Embankment Dams specifies that Simplified Bishop's method would be associated with an allowable factor of safety 10% higher than that associated with Swedish method [19].

Since the conventional wedge analysis method and 'pure friction approach' are still the standard design approaches in dam engineering, all wedges in the ship lock with insufficient factors of safety by the traditional method were reinforced. Table 6 shows that if the generalized method were used, some of the cases would have had no need for reinforcement.

6. Conclusions

The main findings of this paper can be summarized as follows:

(1) A generalized limit equilibrium analysis method for tetrahedral rock wedge stability analysis has been proposed. The main formulation includes:

- establishing a wedge displacement $\boldsymbol{m}$ that inclines at ρ_l and ρ_r to the left and right planes respectively;
- determining the directions of the shear forces applied on the failure planes based on the 'concept of identical shear directions';
- representing all the forces applied on the wedge by the linear combinations of $\boldsymbol{m}$ and the inward normals $\boldsymbol{n}_l$ and $\boldsymbol{n}_r$;
- establishing the force equilibrium equation by projecting all the forces on an axis that is perpendicular to both the left and right 'combined friction forces'. This allows the elimination of all the six unknown components of the two 'combined friction forces'.

The principles in Vector Analysis [Eqs. (17)–(21)] have made it possible to reach a governing equation Eq. (38), from which the factor of safety is solved.

(2) It has been found that the case $\rho_l = 0$ and $\rho_r = 0$ is associated with the conventional wedge stability analysis method which involves an assumption that the shear forces applied on the failure planes are parallel to the line of intersection. It normally gives a smallest F, designated F_c. Another case, associated with $\rho_l = \phi_{el}$ and $\rho_r = \phi_{er}$, which implies that the wedge moves in a direction required by a Mohr–Coulomb's associative flow material, gives an upper bound solution, designated F_u.

(3) A mathematical demonstration is presented to confirm that F obtains its maximum at $\rho_l = \phi_{el}$ and $\rho_r = \phi_{er}$ provided that the conditions of physical admissibility illustrated in Sections 3.1 are not violated. This fact indicates that if Mohr–Coulomb's associative flow law applies, a wedge would indeed fail when the maximum resistance is developed, as proposed by Pan's principle of maximum.

(4) The results obtained from the test problems and case study show that the difference between F_c and F_u is not substantial if the shear strength of the failure planes involves a reasonable value of cohesion. F_c can be considerably lower than F_u if the material is purely frictional. The example of the Three Gorges ship lock gives an appreciation of what the economical impact the generalized solution can bring.

Obviously our profession will not replace the traditional solution with a more optimistic assessment of the stability status of a wedge until more evidence from case studies and physical model testing has confirmed the theory and made it widely accepted. However, a challenge to the conventional approach has been raised and further study on this subject is of both theoretical and practical significance.

Acknowledgements

This work is supported by China National Natural Science Foundation (Contract Number: 50179039).

Appendix A. Reducing the generalized solutions to the special cases

This section demonstrates that Eq. (38) is reducible to two special methods documented in the literatures [1,6].

1. The traditional method

(1) *The original presentations of the solution*. The conventional rock wedge analysis method assumes that the shear forces on the left and right failure planes are parallel to $\boldsymbol{j}$, the line of intersection. By projecting all the forces on the plane perpendicular to $\boldsymbol{j}$, it is possible to avoid the two unknown shear forces and obtain the effective normal forces $\boldsymbol{N}_l$ and $\boldsymbol{N}_r$ applied on the left and right planes, respectively. Hoek and Bray [1] provided the relevant equations that can be rewritten in the following vector analysis form:

$$N_l = (\cos\theta \boldsymbol{w}\cdot\boldsymbol{n}_r - \boldsymbol{w}\cdot\boldsymbol{n}_l)\,\mathrm{cosec}^2\,\theta W, \tag{A.1}$$

$$N_r = (\cos\theta \boldsymbol{w}\cdot\boldsymbol{n}_l - \boldsymbol{w}\cdot\boldsymbol{n}_r)\,\mathrm{cosec}^2\,\theta W. \tag{A.2}$$

The force equilibrium condition in the direction of line of intersection of the planes gives

$$N_l\tan\phi_{el} + N_r\tan\phi_{er} + c_{el}A_l + c_{er}A_r = W\boldsymbol{w}\cdot\boldsymbol{j}. \tag{A.3}$$

The factor of safety F is involved in the subscripts 'e', defined by Eqs. (1) and (2).

(2) *The reduced generalized solutions*. We know that in the conventional method, ρ_l and ρ_r are zero. By substituting these conditions into Eq. (38), we have

$$-c_{el}A_l - c_{er}A_r + (\tan\phi_{el}b_w + \tan\phi_{er}\cdot c_w + a_w)W = 0. \tag{A.4}$$

From Eqs. (26), (28), (29) and (31), we have

$$a_m = 1, \tag{A.5}$$

$$a_w = \boldsymbol{w}\cdot\boldsymbol{j}, \tag{A.6}$$

$$b_w = (\boldsymbol{w}\cdot\boldsymbol{n}_l - \boldsymbol{w}\cdot\boldsymbol{n}_r\cos\theta)\,\mathrm{cosec}^2\,\theta, \tag{A.7}$$

$$c_w = (\boldsymbol{w}\cdot\boldsymbol{n}_r - \boldsymbol{w}\cdot\boldsymbol{n}_l\cos\theta)\,\mathrm{cosec}^2\,\theta. \tag{A.8}$$

Eq. (A.4) becomes

$$c_{el}A_l + c_{er}A_r - [\tan\phi_{el}(\boldsymbol{w}\cdot\boldsymbol{n}_l - \boldsymbol{w}\cdot\boldsymbol{n}_r\cos\theta) + \tan\phi_{er} \times (\boldsymbol{w}\cdot\boldsymbol{n}_r - \boldsymbol{w}\cdot\boldsymbol{n}_l\cos\theta)]W\,\mathrm{cosec}^2\,\theta = a_w W. \tag{A.9}$$

It is not difficult to show that Eq. (A.9) is identical to Eq. (A.3).

2. The upper bound approach

(1) *The original presentations of the solution*. Based on the Upper Bound Theorem of Plasticity, Chen et al. [6] provide a solution to factor of safety by solving the following equation:

$$c_{er}A_r\cos\phi_{er} + c_{el}A_l\cos\phi_{el} = W\boldsymbol{w}\cdot\boldsymbol{v}, \tag{A.10}$$

where $\boldsymbol{v}$ is the unit vector of a plastic velocity that inclines at ϕ_{el} and ϕ_{er} to the left and right planes, respectively. In this paper $\boldsymbol{v}$ is referred to as $\boldsymbol{m}$ (refer to Fig. 5). The left-hand side of Eq. (A.10) refers to the energy dissipation developed on the failure planes, while the right-hand side refers to the work done by external loads. From Fig. 5 it can be found that if ρ_l and ρ_r are equal to ϕ_l and ϕ_r, respectively, $\boldsymbol{P}_l$ and $\boldsymbol{P}_r$ are perpendicular to $\boldsymbol{m}$ and therefore would not contribute to the energy dissipation.

$\boldsymbol{m}$ can be uniquely determined by solving the following equations:

$$\boldsymbol{m} \cdot \boldsymbol{n}_{\mathrm{l}} = \sin \phi_{\mathrm{l}}, \tag{A.11}$$

$$\boldsymbol{m} \cdot \boldsymbol{n}_{\mathrm{r}} = \sin \phi_{\mathrm{r}}. \tag{A.12}$$

(2) *The reduced generalized solutions*. We know that in the upper bound method, $\rho_{\mathrm{l}} = \phi_{\mathrm{el}}$ and $\rho_{\mathrm{r}} = \phi_{\mathrm{er}}$. By substituting these conditions into Eq. (38), one obtains

$$-\cos \phi_{\mathrm{el}} c_{\mathrm{el}} A_{\mathrm{l}} - \cos \phi_{\mathrm{er}} c_{\mathrm{er}} A_{\mathrm{r}} + (\sin \phi_{\mathrm{el}} b_w + \sin \phi_{\mathrm{er}} \cdot c_w + a_w) W = 0. \tag{A.13}$$

From Eq. (9) we have [refer to Eq. (A.11) and (A.12)]

$$\sin \phi_{\mathrm{el}} b_w + \sin \phi_{\mathrm{er}} \cdot c_w + a_w = \boldsymbol{w} \cdot \boldsymbol{m} = \boldsymbol{w} \cdot \boldsymbol{v}. \tag{A.14}$$

Eq. (A.13) then reduces to Eq. (A.10).

References

[1] Hoek E, Bray JW. Rock slope engineering. The Institute of Mining and Metallurgy; 1977.

[2] Londe P, Vigier G, Vormeringer R. The stability of rock slopes, a three dimensional study. J Soil Mech Found Div 1970;6(SM4):1411–34.

[3] Wittke WW. Method to analyse the stability of rock slopes with and without additional loading. Felsmechanik und Ingenieurgeogie 1970;30(Suppl 11):52–79 [in German].

[4] Pan JZ. Stability analyses of structures and landslides. Beijing: Water Resources and Hydropower Press; 1978 [in Chinese].

[5] Chen ZY. Demonstration of 'Pan's principles of maximum and minimum'. Journal of Tsinghua University 1998;1:6–13 [in Chinese].

[6] Chen ZY, Wang YJ, Wang XG, Wang J. An upper bound wedge failure analysis method. Proceedings of the International Symposium on Slope Stability Analysis, vol. I. Mastuyama: Balkema; 1999. p. 325–8.

[7] Sarma KS. Stability analysis of embankments and slopes. J Geotech Am Soc Civ Eng 1979;105(12):1511–24.

[8] Chen ZY, Wang XG, Haberfield C, Yin J, Wang Y. A three-dimensional slope stability analysis method using the upper bound theorem, Part I: theory and methods. Int J Rock Mech Mining Sci 2001;38:369–78.

[9] Drescher A, Kang Y. Kinematic approach to limit load for steady penetration in rigid-plastic soils. Geotechnique 1987;37(3): 233–46.

[10] Chen WF. Limit analysis and soil plasticity. New York: Elsevier; 1975.

[11] Michalowski RL. Three-dimensional analysis: of locally loaded slopes. Geotechnique 1989;39(1):27–38.

[12] Lin M, Drescher A. Limit load in steady 3-D plastic flow around obstacles. In: Pietruszczak S, Pande GN, editors. Numerical models in geomechanics, NUMOG III. Amsterdam: Elsevier; 1989. p. 297–304.

[13] Bishop AW. The use of the slip circle in the stability analysis of slopes. Geotechnique 1955;5(1):7–17.

[14] Morgenstern NR, Price V. The analysis of the stability of general slip surface. Geotechnique 1965;1(15):79–93.

[15] Fellenius W. Erdstatisch Berechnungen (revised ed.). Berlin: W. Ernst und Sohn; 1939.

[16] Duncan JM. State of the art: limit equilibrium and finite element analysis of slopes. J Geotech Eng 1996;122(7):577–96.

[17] Whitman RV, Bailey W. Use of computers for slope stability analysis. ASCE JSMFE 1967;93(4):475–98.

[18] Chen ZY. Soil slope stability analysis—theory, methods and computer programs. China: China Water Resources Press Beijing; 2003 [in Chinese].

[19] Ministry of Water Resources of China. Design codes for embankment dams, 1984. SDJ 218-84.